NASA Technical Memorandum 86912
AIAA-85-0380

Analytical Modeling of Circuit Aerodynamics in the New NASA Lewis Altitude Wind Tunnel

Charles E. Towne, Louis A. Povinelli, William G. Kunik,
Kenneth K. Muramoto, and Christopher E. Hughes
Lewis Research Center
Cleveland, Ohio

and

Ralph Levy
Scientific Research Associates
Glastonbury, Connecticut

Prepared for the
Twenty-third Aerospace Sciences Meeting
sponsored by the American Institute of Aeronautics and Astronautics
Reno, Nevada, January 14–17, 1985

NASA

1 Report No	2 Government Accession No	3 Recipient's Catalog No
NASA TM-86912 AIAA-85-0380		

4 Title and Subtitle

Analytical Modeling of Circuit Aerodynamics in the New NASA Lewis Altitude Wind Tunnel

5 Report Date

6 Performing Organization Code

505-40-74

7 Author(s)

Charles E. Towne, Louis A. Povinelli, William G. Kunik, Kenneth K. Muramoto, Christopher E. Hughes, and Ralph Levy

8 Performing Organization Report No

E-2405

10 Work Unit No

9 Performing Organization Name and Address

National Aeronautics and Space Administration
Lewis Research Center
Cleveland, Ohio 44135

11 Contract or Grant No

13 Type of Report and Period Covered

Technical Memorandum

12 Sponsoring Agency Name and Address

National Aeronautics and Space Administration
Washington, D.C. 20546

14 Sponsoring Agency Code

15 Supplementary Notes

Charles E. Towne, Louis A. Povinelli, William G. Kunik, Kenneth K. Muramoto, and Christopher E. Hughes, NASA Lewis Research Center; Ralph Levy, Scientific Research Associates, P.O. Box 498, Glastonbury, Connecticut 06033. Prepared for the Twenty-third Aerospace Sciences Meeting sponsored by the American Institute of Aeronautics and Astronautics, Reno, Nevada, January 14-17, 1985.

16 Abstract

An extensive analytical and experimental modeling effort is underway at NASA Lewis Research Center as part of the program to rehabilitate and extend the capability of the Altitude Wind Tunnel (AWT). The analytical modeling program involves the use of advanced axisymmetric and three-dimensional viscous analyses to compute the flow through the various AWT components. In this paper, results obtained to date are presented for the analytical modeling of the high speed leg aerodynamics. These include an evaluation of the flow quality at the entrance to the test section, an investigation of the effects of test section bleed for different model blockages, and an examination of three-dimensional effects in the diffuser due to reentry flow and due to the change in cross-sectional shape of the exhaust scoop.

17 Key Words (Suggested by Author(s))	18 Distribution Statement
Wind tunnel modeling; Analytical modeling; Viscous analysis; Altitude Wind Tunnel	Unclassified - unlimited STAR Category 02

19 Security Classif (of this report)	20 Security Classif (of this page)	21 No of pages	22 Price*
Unclassified	Unclassified		

*For sale by the National Technical Information Service, Springfield, Virginia 22161

ANALYTICAL MODELING OF CIRCUIT AERODYNAMICS IN THE NEW NASA LEWIS ALTITUDE WIND TUNNEL

Charles E. Towne, Louis A. Povinelli, William G. Kunik,
Kenneth K. Muramoto, and Christopher E. Hughes
National Aeronautics and Space Administration
Lewis Research Center
Cleveland, Ohio 44135

and

Ralph Levy
Scientific Research Associates
Glastonbury, Connecticut 06033

Abstract

An extensive analytical and experimental modeling effort is underway at NASA Lewis Research Center as part of the program to rehabilitate and extend the capability of the Altitude Wind Tunnel (AWT). The analytical modeling program involves the use of advanced axisymmetric and three-dimensional viscous analyses to compute the flow through the various AWT components. In this paper, results obtained to date are presented for the analytical modeling of the high speed leg aerodynamics. These include an evaluation of the flow quality at the entrance to the test section, an investigation of the effects of test section bleed for different model blockages, and an examination of three-dimensional effects in the diffuser due to reentry flow and due to the change in cross-sectional shape of the exhaust scoop.

E-2405

Introduction

An effort is currently underway at the NASA Lewis Research Center to rehabilitate the Altitude Wind Tunnel (AWT) in order to provide a unique national subsonic propulsion, icing, and aeroacoustic facility. Modifications to be made to the existing tunnel include (1) a new drive motor system, increasing the maximum test section Mach number from around 0.6 to nearly 1.0, (2) the addition of icing and acoustic testing capabilities, (3) a new octagonal test section with longitudinally slotted walls and reentry flaps for boundary layer and model blockage control, (4) an independently powered plenum evacuation system (PES), (5) a new, shorter contraction section, (6) a new tunnel heat exchanger, (7) a new engine exhaust removal scoop, and (8) new turning vanes. An description of the capabilities of the new tunnel is presented by Chamberlin and Miller,[1] and details on its use for icing research are presented by Blaha and Shaw.[2]

As part of this effort, intensive experimental and analytical modeling programs have begun at NASA Lewis. The purpose of the modeling work is to assess the performance of the new AWT design, study the inevitable problems that will arise, and investigate proposed design changes. The experimental program will primarily utilize 1/10 scale component and complete loop models. These models will be faithful representations of the full-scale facility, including features such as slotted walls, reentry flaps, and a plenum evacuation system. An overview of the entire modeling effort is presented by Abbott, et al.[3]

The present paper concentrates on the analytical modeling of the aerodynamics in the high speed leg. This effort involves the use of recently developed axisymmetric and three-dimensional analyses to compute and evaluate the flow through the various AWT components.

Wind Tunnel Description

The new Altitude Wind Tunnel is shown in Fig. 1, and compared with the existing tunnel in Fig. 2. The new tunnel differs from the existing tunnel in several respects, especially in the high speed and back legs.

In the settling chamber upstream of the contraction section either a water spray system or a honeycomb/screen combination will be present, depending on whether or not an icing test is being run. The contours of the contraction section itself have been modified to shorten it and eliminate the sharp corner at the inlet. The cross section of the contraction transitions from a circle 51 ft in diameter at the entrance to an octagon with an equivalent diameter of 20 ft at the exit. The contraction ratio is thus 6.5.

The test section has been lengthened from 40 to 55 ft, and the cross section has been changed from circular to octagonal. Although the nominal equivalent diameter of the test section is 20 ft, four of the eight sides diverge slightly to allow for boundary layer growth. Longitudinal bleed slots at the vertices of the octagon are used for boundary layer and model blockage control. Removable inserts allow the porosity to vary from 0.0 to 20.0 percent. The test section is surrounded by a 40 ft diameter plenum. Flow bled off from the test section may thus reenter the tunnel through the downstream end of the slots, or through a set of eight reentry flaps at the entrance to the high speed diffuser. Additional bleed capacity is provided by an independently powered plenum evacuation system (PES). Flow bled off through the PES reenters the tunnel downstream of the fan in the back leg. With the PES, the maximum bleed capacity is about 12 percent of the total tunnel mass flow. The operating envelope for the test section is shown in Fig. 3.

The entrance to the high speed diffuser has been modified to accommodate the reentry flaps, and to change the cross section from octagonal to circular. At the entrance the equivalent radius is 10.0537 ft, and at the exit the radius is 13.5 ft. A new nonremovable engine exhaust scoop has been added to allow testing with an operating engine. A closed scoop tip will be added for non-

propulsion tests. The cross section of the open tipped scoop transitions from a 2.5 ft outside diameter circle at the entrance to a 6.67 by 12.67 ft ellipse at the diffuser exit station. The scoop then continues with a constant cross section straight through the turning vanes and the wall in corner one. Taking the scoop into account, the diffuser area ratio is thus 1.59.

New turning vanes have been designed for all four corners. In corners one and two, downstream of the high speed diffuser, a new low-loss design is being used. In corners three and four, where the velocities will be much lower, a simple circular-arc design is used. The side legs in the new AWT are identical to those in the original tunnel.

The back leg has been completely redesigned. A new drive system increases the maximum test section Mach number from 0.6 to nearly 1.0. Makeup air and the PES air are reinjected into the tunnel in the back leg downstream of the fan. A new "blister" cooler concept has been incorporated into the back leg to accommodate the greater cooling capacity needed in the new tunnel. Immediately downstream of the cooler is an acoustic silencer. For acoustic testing, treatment is also used in the test section, and on the turning vanes in corners three and four.

Analytical Modeling Approach

Because the state-of-the-art in computational fluid mechanics has advanced significantly in the last few years, more sophisticated analyses are available for modeling the AWT than were available for earlier wind tunnels. In the AWT modeling, emphasis has been placed on axisymmetric and three-dimensional viscous analyses. In Table 1 the computer codes used for the various AWT components are listed, along with brief comments about the flow being computed. VISTA[4,5], ADD[6], and PANPER[7] are basically axisymmetric fully viscous "parabolized" Navier-Stokes analyses, although all include swirl. In addition, ADD can include the effects of struts. PANPER is actually a version of the ADD code that includes the effects of a rotating propeller by incorporating a lifting line analysis. NAP[8] and DENTON[9,10] are, respectively, axisymmetric and three-dimensional inviscid Euler analyses. PEPSIG[11-13] and PEPSIM[14] are three-dimensional fully viscous "parabolized" Navier-Stokes analyses. The capabilities of all of these codes have been previously verified and documented by comparison with a variety of benchmark experimental data, so that a high degree of confidence exists in their use.

Note that existing computer codes are being used where possible. However, several modifications to existing codes are also being made to address specific AWT features. In particular, the PEPSIG code is being modified, under contract with Scientific Research Associates, to examine the circular-to-octagonal transition in the contraction section, the slotted wall test section, and the nonaxisymmetric exhaust scoop in the high-speed diffuser.

Computed Results

Contraction Section

One of the first AWT components to be investigated was the contraction section. The most important criteria in assessing contraction section performance is the quality of the flow it delivers to the test section. To quantify this, a distortion parameter was defined as the difference between the maximum and minimum streamwise velocities (outside the boundary layer), nondimensionalized by the area-weighted average velocity. For the M = 0.8 condition, a distortion level less than 2.5 percent was desired. The distortion levels computed using the VISTA code are plotted as a function of nominal test section Mach number in Fig. 4. (Because the modifications to the PEPSIG code needed for the circular-to-octagonal transition are not yet complete, only axisymmetric results are presented here). Values between 1.0 to 1.5 percent are predicted at the contraction section exit, falling to below 0.1 percent 10 ft downstream. These values appear to be independent of tunnel pressure altitude. Also shown in Fig. 4 are the values at the Mach 0.8 condition computed as part of the preliminary engineering study by Sverdrup Technology, Inc.[15], using the method of Reference 16 in an inviscid mode. These values are slightly higher, generally between 1.5 to 2.0 percent at the contraction section exit, but also falling to below 0.1 percent 10 ft downstream.

In the preceding results, the initial boundary layer thickness was two ft. Since the actual value may be different, additional cases were run at the Mach 0.8 and 32 000 ft condition to determine the effect of the initial boundary layer thickness on the distortion level. The results are shown in Fig. 5. Over the range studied, the distortion level is essentially constant.

Another flow quality factor is the boundary layer thickness in the test section. In Fig. 6, boundary layer thickness is plotted as a function of test section Mach number. The altitude conditions along the total temperature limit line in Fig. 3 were used for all Mach numbers. In addition two other altitude conditions were run at the Mach 0.2 and 0.8 conditions. The boundary layer has thinned from 2.0 ft at the contraction section entrance to 0.20 to 0.25 ft at the exit, then increases to 0.35 to 0.40 ft 10 ft downstream. The results are only weak functions of altitude and Mach number. The effect of the initial boundary layer thickness on the final boundary layer thickness is shown in Fig. 7. These results are for the Mach 0.8, 32 000 ft altitude condition. As with the distortion, the final boundary layer thickness is essentially constant.

The above results for distortion and boundary layer thickness indicate that the redesigned contraction section meets the mean flow quality requirements for the new AWT. However, another item of concern is the possibility of flow separation near the inlet to the contraction section. The streamwise velocity profiles computed by the VISTA code for the Mach 0.8, 32 000 ft altitude condition are presented in Fig. 8. Although it can't be seen in the figure, the flow is close to separation near the bellmouth entrance. The profiles downstream are not affected, however, and

the boundary layer becomes much thinner as the flow accelerates.

It is expected that the flow near the contraction inlet will be influenced by the position of the honeycomb/screen combination in the settling chamber. To investigate this, the VISTA code was run starting at different axial stations upstream of the contraction section. These cases were run at the Mach 0.8, 32 000 ft altitude condition, with a 2 ft thick initial boundary layer. The computed skin friction coefficients are plotted as a function of axial distance in Fig. 9. Although no separation was seen in any of these results, the skin friction coefficient does drop to nearly zero. The furthest downstream starting location gave the highest skin friction value, probably because the local adverse pressure gradient in this region had less time to influence the boundary layer. This region will be studied more closely during the physical modeling tests.

Test Section

In the AWT test section, eight longitudinal bleed slots will be used to control the tunnel wall boundary layer and model blockage effects. The goal is to provide an environment for the model in the wind tunnel that is the same as in free flight. Modifications currently being made to the PEPSIG code will allow a detailed three-dimensional analysis of this flow. In this analysis, a pressure boundary condition will be used at the slot locations, and the local bleed rate will be computed. These modifications are not yet complete, however, so the axisymmetric VISTA code is being used in the initial modeling work. With this code, the local bleed rate is specified directly.

Three simple bodies of revolution were used in the analysis to simulate model blockages of 1, 3, and 6 percent. All were 35 ft long with tapered leading and trailing edges. The VISTA code was first used for each model in an external flow mode, with the outer boundary far from the body and with appropriate free stream boundary conditions. The flow conditions corresponded to the Mach 0.8, 32 000 ft altitude point of Fig. 3. This determined the desired free flight environment for each model. Calculations were then made for each model in the AWT test section with various bleed rates. Since the analysis is axisymmetric, the slots could not be modeled three-dimensionally. Instead, porous wall bleed was used, uniformly distributed in the circumferential direction. For simplicity, the bleed was also assumed uniform in the axial direction, although this is not required by the analysis, and was applied over the entire length of the test section.

In Fig. 10 the 6 percent blockage model is shown in the test section, along with the velocity profiles computed for 6 percent total bleed. The results of the bleed study for all three blockage models are summarized in Figs. 11 to 13. Here both static pressure and skin friction coefficient along the centerbody surface are plotted as functions of axial distance for various total bleed rates, and compared with the desired external flow result. The skin friction coefficient appears to be relatively insensitive to the bleed rate, but the static pressure is not. The static pressure in the tunnel matches the external flow results most closely when the total bleed rate matches the centerbody blockage. The match is closer, however, over the front half of the body than the back half. Better agreement with the external flow results could probably be obtained with a proper nonuniform bleed distribution in the axial direction. These results do indicate, however, that bleed can be used to help simulate free flight conditions in the wind tunnel. This problem will be studied further using the modified PEPSIG code, as well as in the physical modeling tests.

One of the important uses of the new Altitude Wind Tunnel will be testing of high speed turboprops. A typical example of an advanced turboprop configuration is shown in Fig. 14. The PANPER code was used to perform a bleed study similar to the one done with the VISTA code, but including the effects of a rotating propeller. The propeller is modeled using a lifting line analysis and, since the code is axisymmetric, averaging the results in the circumferential direction. The configuration actually modeled in this study included the propeller and the nacelle as far downstream as the supporting strut shown in Fig. 14. Blockages of 0.86, 2.0, 4.0, and 6.0 percent were used, corresponding to propeller diameters of 5.22, 7.96, 11.28, and 13.80 ft, respectively. The Mach 0.8, 32 000 ft altitude condition was again used as the operating point.

For the turboprop model, the apparent efficiency of the propeller was used as the criterion for determining when free stream conditions were being properly simulated in the wind tunnel. In this study, the different blockage models were geometrically similar, and therefore the computed free stream efficiency was the same for each model, about 0.78. The results of the bleed study are shown in Fig. 15, where the computed apparent efficiency is plotted as a function of bleed rate for the four different blockages and for external flow. As in the bleed study using VISTA, the bleed was applied uniformly in both the circumferential and axial directions, and over the entire length of the test section. As shown in the figure, the two lower blockages reach the free stream efficiency level with about 4.0 and 6.5 percent bleed, respectively. For the two higher blockages the efficiency also increases with bleed rate. However, results are shown only up to 8.0 percent bleed because of difficulties encountered in running the code at higher bleed rates. Note that the bleed rates needed to simulate free stream propeller efficiency in this study are considerably higher than those needed to simulate free stream pressure levels along a simple centerbody model in the study using the VISTA code. As in that study, however, these results do indicate that bleed can be used to help simulate free stream conditions in the wind tunnel. The actual amount and distribution of bleed that will be needed will be studied further in the physical modeling tests, and in the calibration of the tunnel itself.

High Speed Diffuser

When bleed is used in the AWT test section, at least some of the flow bled off will reenter

the tunnel through a set of eight reentry flaps at the entrance to the high speed diffuser. Thus the inlet flow to the diffuser will be distorted in the circumferential direction. The PEPSIM code was used to examine the effect of this inlet distortion on the flow downstream. Although the PEPSIM code computes three-dimensional flow, the geometry must be axisymmetric. The exhaust scoop, which actually transitions from a circular to elliptical cross section, was therefore treated as an axisymmetric centerbody with the proper area variation. The octagonal to circular transition of the outer wall was also not modeled.

The flow at the diffuser inlet is shown in Fig. 16(a) in the form of streamwise velocity contours and secondary velocity vectors. The flow conditions correspond to the Mach 0.8, 32 000 ft altitude condition in the test section. Thin boundary layers were specified on the outer wall, because of bleed in the test section, and on the centerbody, because its leading edge is near the diffuser inlet. Low velocity pockets were placed at the locations of the reentry flaps. The size of these pockets was estimated from the reentry flap geometry, and initial velocity profiles were specified using the data of Reference 17 as a guide. The computed results at the diffuser exit are presented in Fig. 16(b). Although the basic distortion pattern is still evident, the gradients have lessened due to diffusion and viscous mixing.

In Fig. 17, the PEPSIM results are shown for a similar case with swirl. The secondary velocity pattern at the initial station represents that produced by a 13 ft diameter propeller in the test section. The swirl velocity was 16 percent of the axial velocity. As shown in Fig. 17(b), the primary effect of swirl is a shift in the distortion pattern in the circumferential direction. The circumferential gradient of the streamwise velocity steepens on one side of the low velocity regions and lessens on the other. These two calculations indicate that the distortion at the diffuser inlet caused by flow through the reentry flaps does not cause significant problems downstream. However, the initial flow profiles were estimates only. Further analysis may be done after these profiles are measured in the physical modeling tests.

Another item of concern in the high speed diffuser is the cross section transitioning of the exhaust scoop from circular to elliptical. The PEPSIG code, modified to compute the three-dimensional flow through ducts with this type centerbody, was used to investigate this problem. In this study, the transition of the outer wall from octagonal to circular was not modeled.

In Fig. 18 the flow development through the diffuser is presented in the form of axial velocity contours at six stations through the duct. The results at the exit station are shown at a larger scale in Fig. 19, where the contour values are normalized by the nominal free stream velocity at the diffuser inlet. The flow conditions used in this calculation correspond to the Mach 0.8, 32 000 ft altitude condition in the test section. At the first three stations the scoop is circular, and the flow is essentially axisymmetric. The boundary layers grow thicker along both surfaces. About halfway through the duct the scoop cross section starts to transition to an ellipse. The scoop boundary layer becomes thinner on the sides, and thicker on the top and bottom. The three-dimensional effects are primarily confined to the scoop boundary layer, with the outer wall boundary layer remaining nearly axisymmetric. No separation is predicted in this calculation. However, it's possible that separation could occur along the top and bottom of the scoop, or on the outer wall, when the relatively low energy boundary layer hits the local adverse pressure gradient near the leading edge of the corner turning vanes. This area will be examined in the physical modeling tests.

Concluding Remarks

An extensive analytical modeling program is underway at NASA Lewis Research Center, in which advanced axisymmetric and three-dimensional viscous analyses are being used to evaluate the design of the new Altitude Wind Tunnel. Based on the results obtained to date, the following conclusions may be drawn.

1. The quality of the flow at the test section entrance is good, with distortion levels below 2.0 percent at the contraction exit and below 0.1 percent 10 ft downstream. The boundary layer thickness at the contraction exit is less than 3.0 in, increasing to about 4.5 in (without bleed) 10 ft downstream.

2. The flow is close to separation at the inlet to the contraction section. If in reality the flow does separate, the separation region should be small.

3. Bleed can be used to help simulate free flight conditions in the wind tunnel. The amount of bleed required is a function of model blockage.

4. The distortion at the high speed diffuser entrance, produced by low velocity flow through the reentry flaps, causes no significant problems downstream.

5. The three-dimensional effects generated by the exhaust scoop transition from circular to elliptical are primarily confined to the scoop boundary layer. The diffuser itself does not separate (at least at Mach 0.8 and 32 000 ft). However, the boundary layers on the top and bottom of the scoop, and on the diffuser outer wall, are such that the possibility of separation exists near the leading edge of the corner turning vanes.

The analytical modeling work on AWT at NASA Lewis is continuing. Areas still to be examined include the three-dimensional effects of the longitudinal slots in the test section, the circular to octagonal transition in the contraction section, total pressure losses through the various AWT components, and loads on the surfaces.

References

1. Miller, B.A., and Chamberlin, R., "Altitude Wind Tunnel (AWT) - A Unique Facility for Propulsion System and Adverse Weather Testing," AIAA Paper 85-0314, Jan. 1985.

2. Blaha, B., and Shaw, R.J., "The NASA Altitude Wind Tunnel: Its Role in Advanced Icing Research and Development," AIAA Paper 85-0090, Jan. 1985.

3. Abbott, J.M., Diedrich, J.H., Groeneweg, J.F., Povinelli, L.A., Reid, L., Reinmann, J.J., and Szuch, J.R., "Analytical and Physical Modeling Program for the NASA Lewis Research Center's Altitude Wind Tunnel (AWT)," AIAA Paper 85-0379, Jan. 1985.

4. Towne, C.E., and Hoffman, J.D., "Computation of Viscous Flow in Planar and Axisymmetric Ducts by an Implicit Marching Procedure," AIAA Paper 84-0256, Jan. 1984.

5. Towne, C.E., and Hoffman, J.D., "Implicit Marching Solution of Compressible Viscous Subsonic Flow in Planar and Axisymmetric Ducts," NASA TM-82876, 1982.

6. Anderson, O.L., Hankins, G.B., and Edwards, D.E., "User's Manual for Axisymmetric Diffuser Duct (ADD) Code," Vols. 1-3, United Technologies Corp., East Hartford, CT, UTRC81-65-VOL-1,-VOL-2,-VOL 3; Feb. 1982. (NASA CR-165598-VOL-1,-VOL-2,-VOL-3)

7. Egolf, T.A., Anderson, O.L., Edwards, D.E., and Landgrebe, A.J., "An Analysis for High Speed Propeller-Nacelle Aerodynamic Performance Prediction," Vols. 1-2, United Technologies Research Center, East Hartford, CT, UTRC Report R79-912949-19-VOL-1,-VOL-2; June 1979. (NASA CR-169450, NASA CR-169451)

8. Cline, M.C., "Computation of Steady Nozzle Flow by a Time-Dependent Method," AIAA Journal, Vol. 12, No. 4, Apr. 1974, pp. 419-420.

9. Denton, J.D., "Extension of the Finite Area Time Marching Method to Three-Dimensions," in Transonic Flows in Axial Turbomachinery, Vol. 1, Von-Karman Institute of Fluid Dynamics, Lecture Series 84, Von-Karman Institute of Fluid Dynamics, 1976.

10. Denton, J.D., "Time Marching Methods for Turbomachinery Flow Calculations," in Numerical Methods in Applied Fluid Dynamics, edited by B. Hunt, Academic Press, 1980, pp. 473-493.

11. Briley, W.R., and McDonald, H., "Analysis and Computation of Viscous Subsonic Primary and Secondary Flows," in Computational Fluid Dynamics Conference, AIAA, 1979, pp. 74-88.

12. Levy, R., McDonald, H., Briley, W.R., and Kreskovsky, J.P., "A Three-Dimensional Turbulent Compressible Subsonic Duct Flow Analysis for Use with Constructed Coordinate Systems," AIAA Paper 80-1398, July 1980.

13. Levy, R., Briley, W.R., and McDonald, H., "Viscous Primary/Secondary Flow Analysis for Use with Nonorthogonal Coordinate Systems," AIAA Paper 83-0556, Jan. 1983.

14. Lin, Shyi-Jang, Kreskovsky, J.P., Briley, W.R., and McDonald, H., "Further Development of a Method for Computing Three-Dimensional Subsonic Flows in Turbofan Lobe Mixers," Scientific Research Associates, Glastonbury, CT, R83-900011-F, Nov. 1983. (NASA CR-168304)

15. Davis, M.W., Martindale, W.R., and Boylan, D.E., "Aerodynamic Design of Test Section Contraction for 20-Foot AWT," Report 8816-B21-044-20, Sverdrup Technology, Jan. 1984.

16. Cline, M.C., "VNAP - A Computer Program for Computation of Two-Dimensional, Time-Dependent Compressible, Viscous, Internal Flow," Los Alamos Scientific Laboratory, Report LA-7326, Nov. 1978.

17. Bergeles, G., Gosman, A.D., and Launder, B.E., "Near-Field Character of a Jet Discharged Through a Wall at 30 Degrees to a Mainstream," AIAA Journal, Vol. 15, No. 4, Apr. 1977, pp. 499-504.

TABLE 1 - ANALYTICAL MODELING OF AWT CIRCUIT AERODYNAMICS

Component	Code	Comments
Contraction	VISTA, ADD	Axisymmetric flow
	PEPSIG	Three-dimensional, transition to octagon
Test Section	VISTA, ADD	Axisymmetric flow, uniform bleed
	PANPER	Axisymmetric flow, uniform bleed, effects of rotating propeller
	DENTON	Three-dimensional inviscid flow, circular cross section, rotating propeller
	PEPSIG	Three-dimensional, circular cross section, slotted walls
High-speed diffuser	VISTA, ADD	Axisymmetric flow, swirl
	NAP	Axisymmetric inviscid flow, effects of acoustic choke
	PEPSIM	Three-dimensional, circular cross section, distortion due to reentry flaps
	PEPSIG	Three-dimensional, nonaxisymmetric centerbody
Back leg	VISTA, ADD	Axisymmetric flow, swirl
	PEPSIM	Three-dimensional, circular cross section, distortion due to PES reentry
Side legs	VISTA, ADD	Axisymmetric flow
	PEPSIG	Three-dimensional, distorted inlet profile

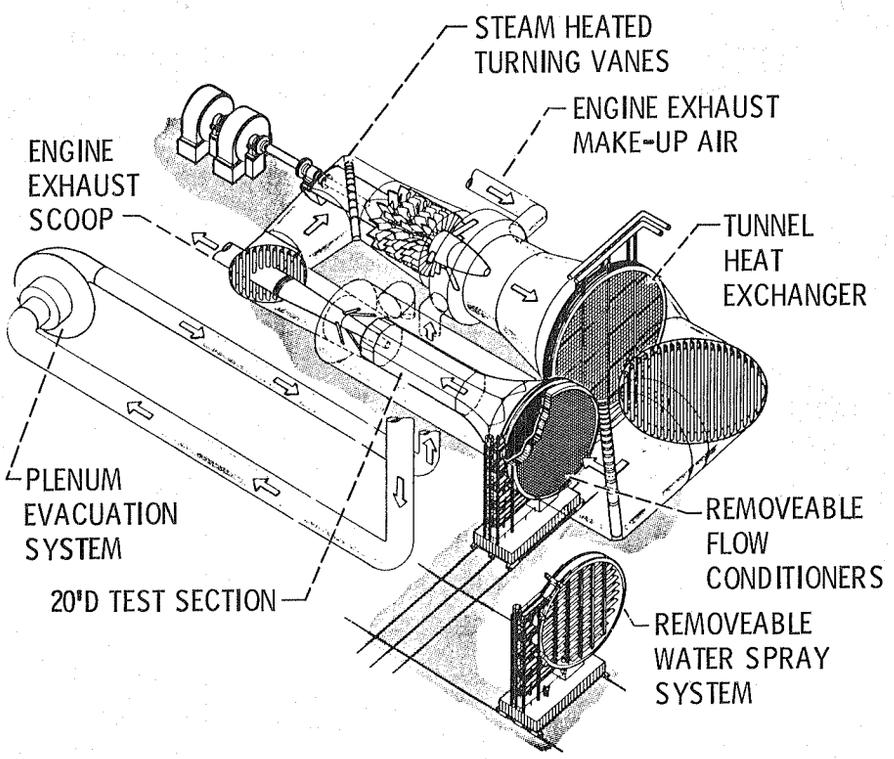

Figure 1. - The new NASA Lewis altitude wind tunnel (AWT).

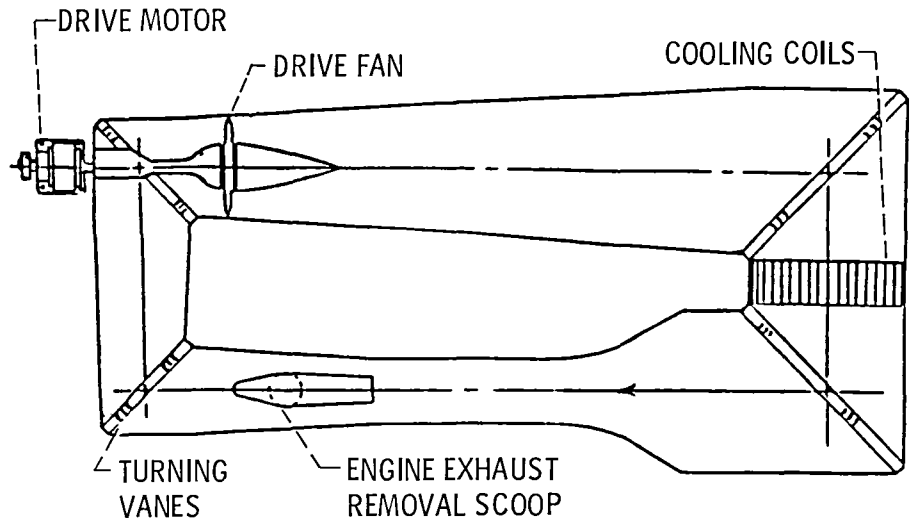

(a) Existing tunnel.

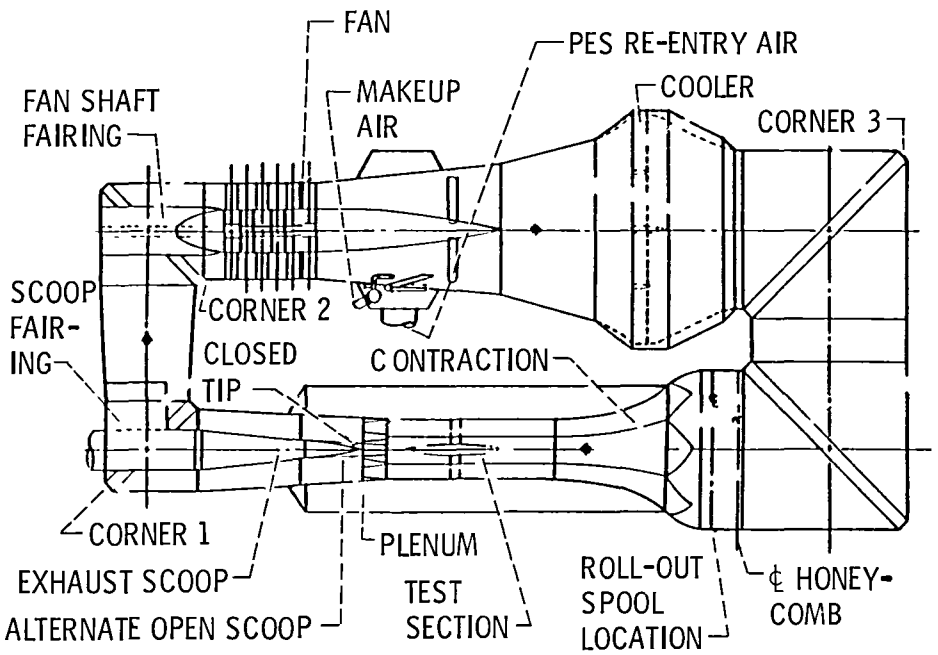

(b) New tunnel.

Figure 2. - Comparison of existing and new NASA Lewis altitude wind tunnel configurations.

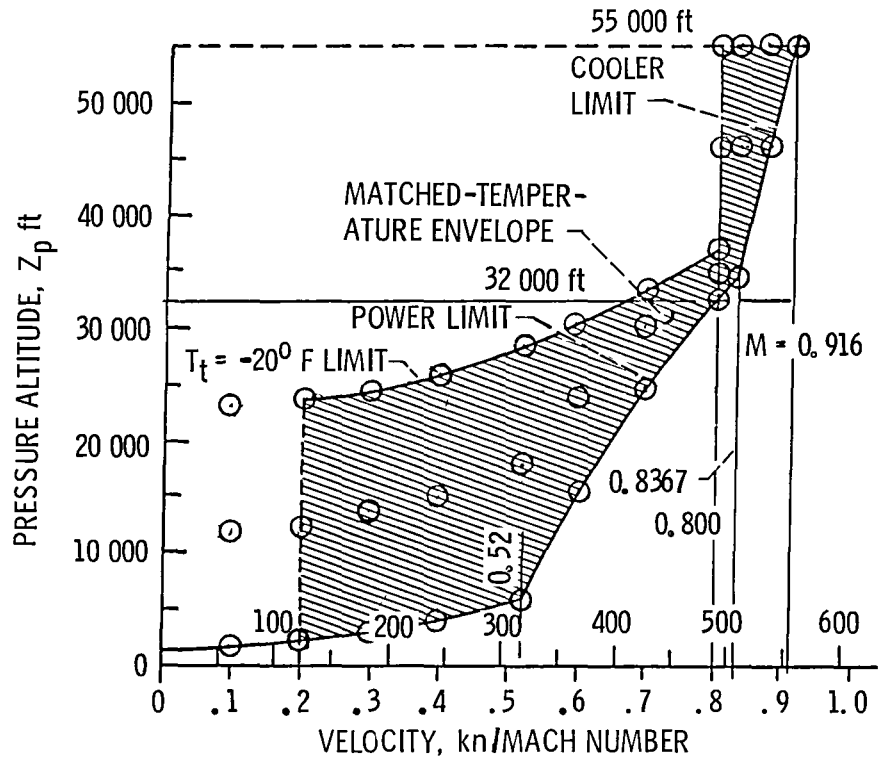

Figure 3. - Operating envelope for AWT test section.

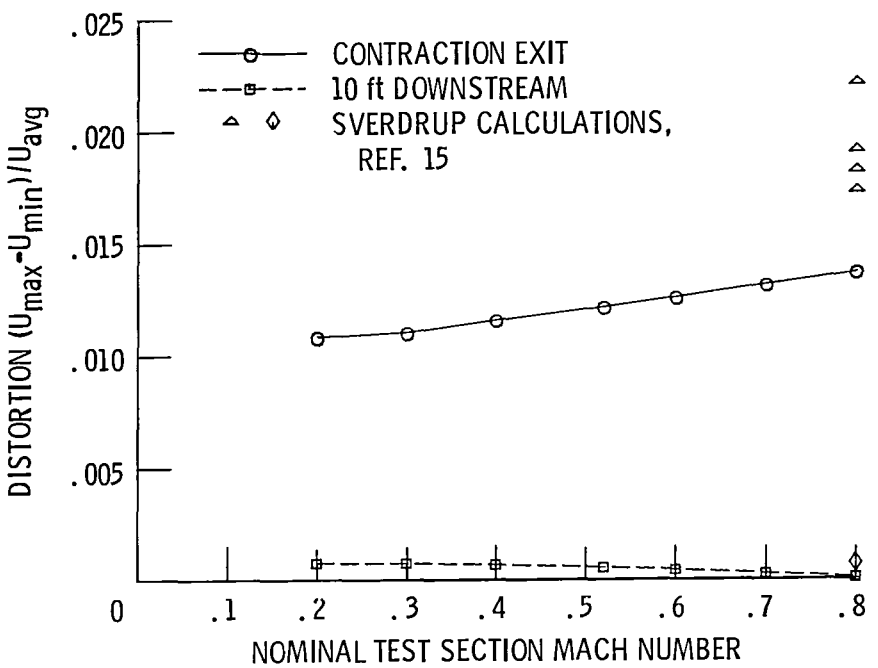

Figure 4. - Effect of test section Mach number on distortion.

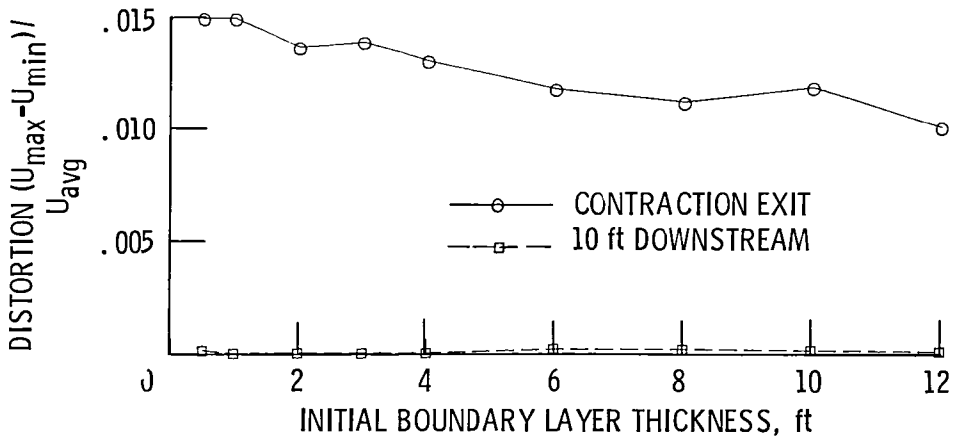

Figure 5. - Effect of contraction inlet boundary layer thickness on test section distortion.

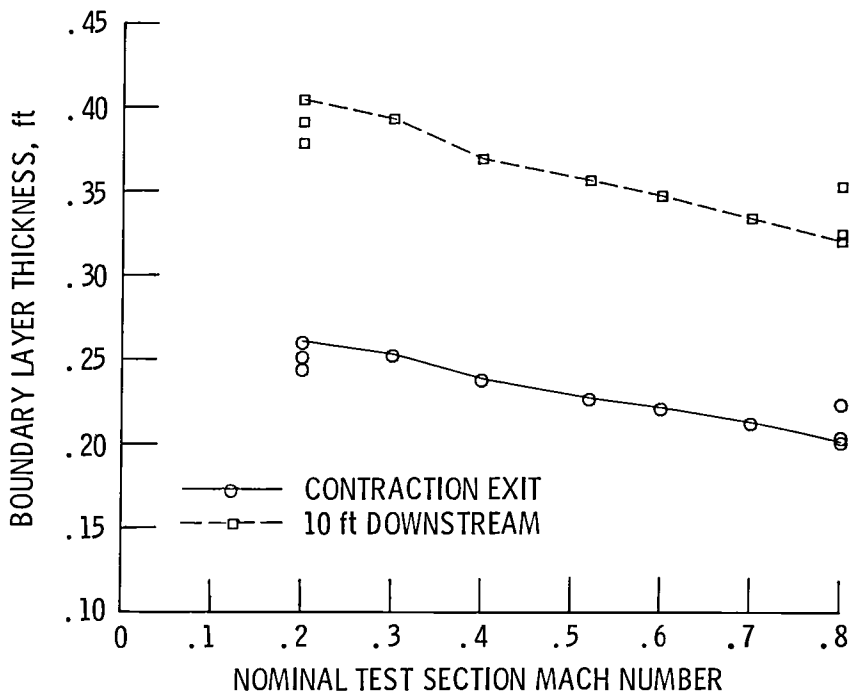

Figure 6. - Effect of test section Mach number on test section boundary layer thickness.

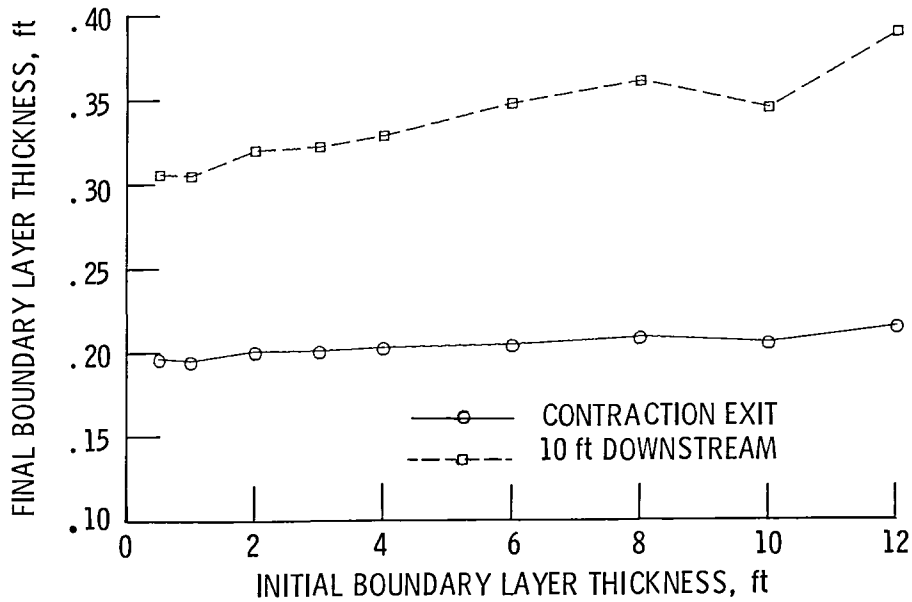

Figure 7. - Effect of contraction inlet boundary layer thickness on test section boundary layer thickness.

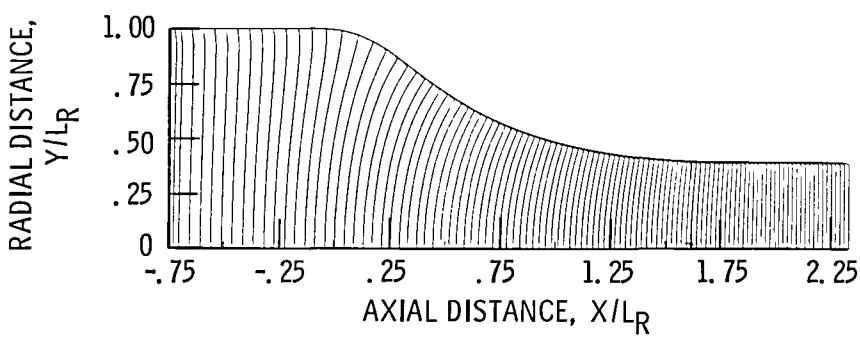

Figure 8. - Computed streamwise velocity profiles in AWT contraction section.

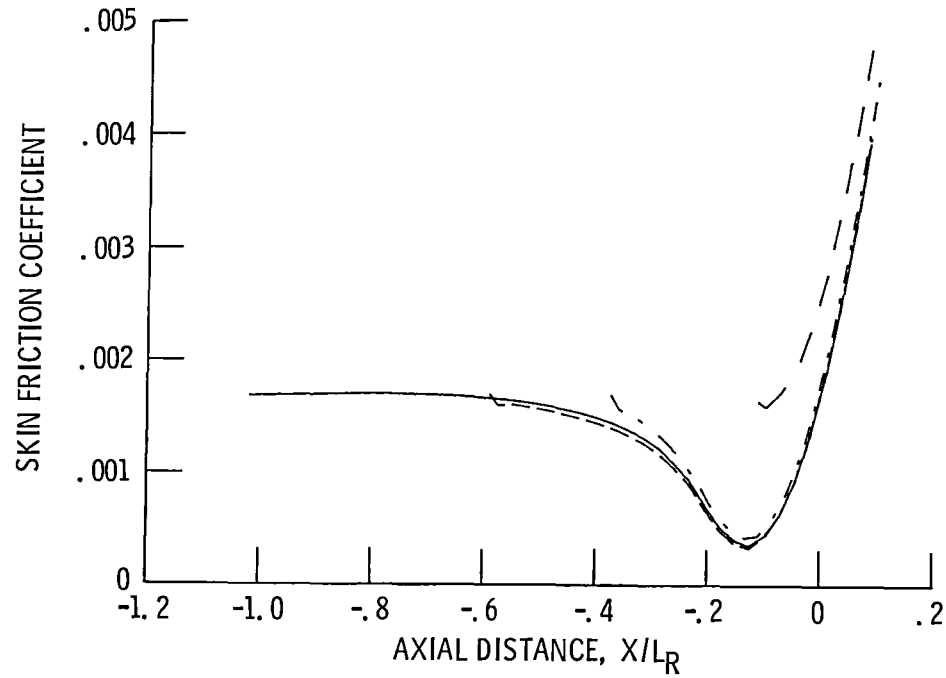

Figure 9. - Effect of starting location on skin friction distribution near contraction inlet.

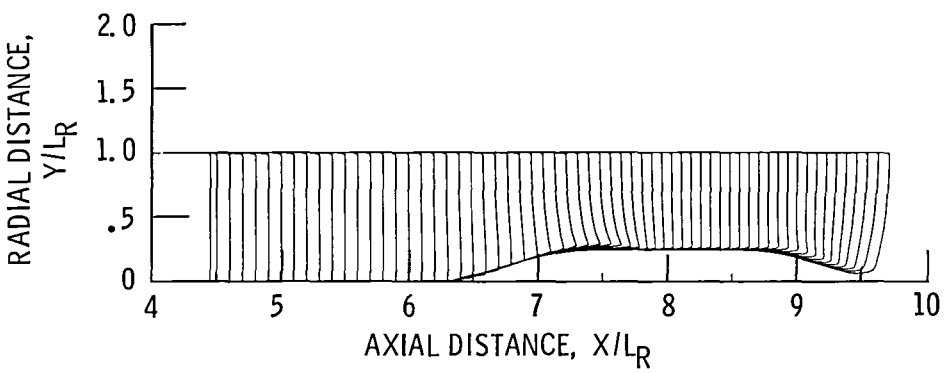

Figure 10. - Computed streamwise velocity profiles in AWT test section. Blockage, 6 percent.

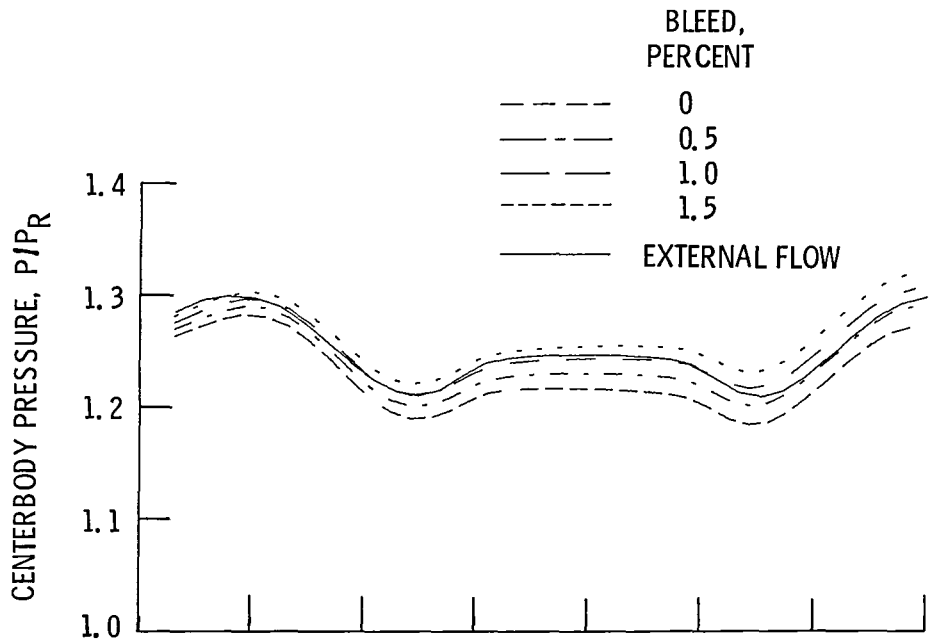

(a) Static pressure.

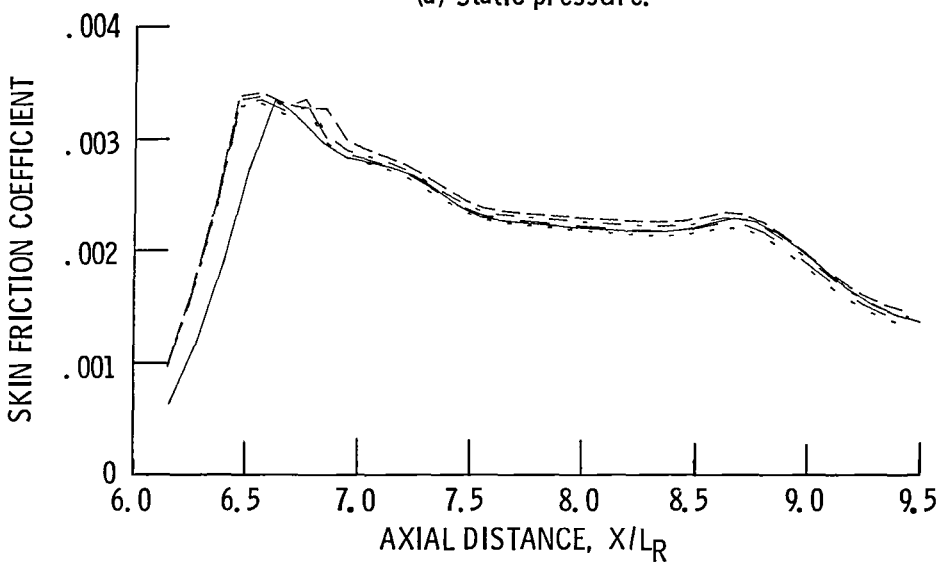

(b) Skin friction coefficient.

Figure 11. - Effect of mass flow removal in AWT test section for 1% blockage, Mach 0.8, 32 000 ft.

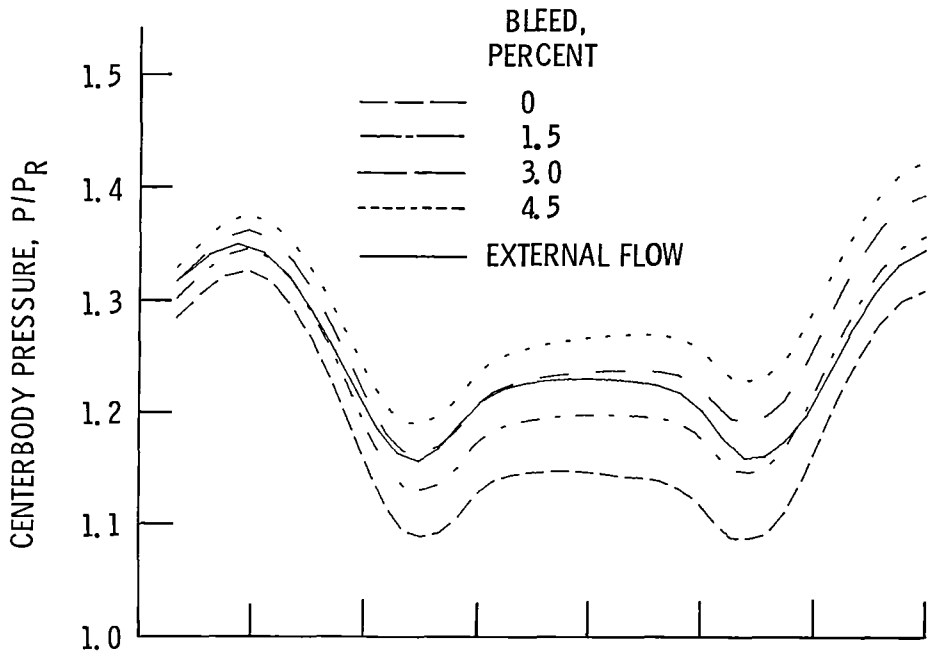

(a) Static pressure.

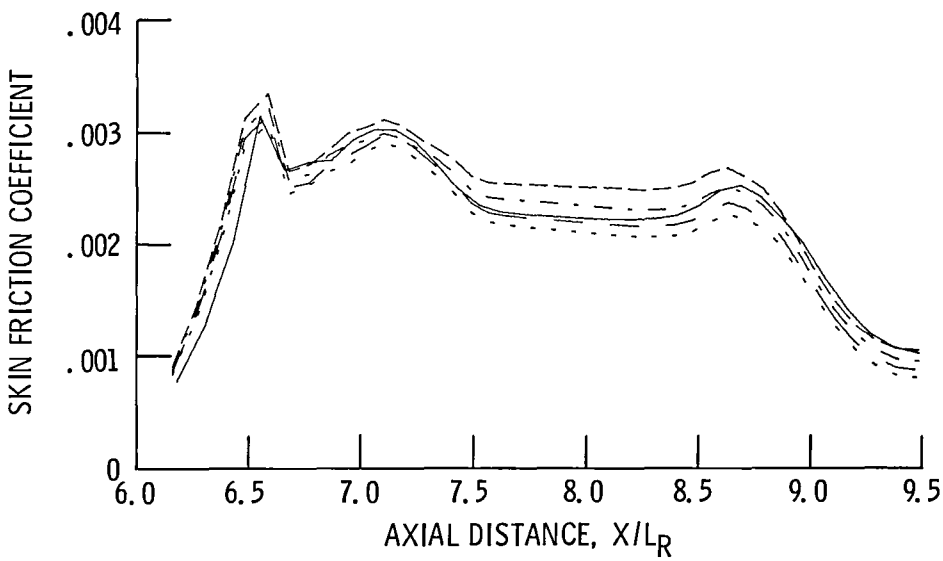

(b) Skin friction coefficient.

Figure 12. - Effect of mass flow removal in AWT test section for 3% blockage, Mach 0.8, 32 000 ft.

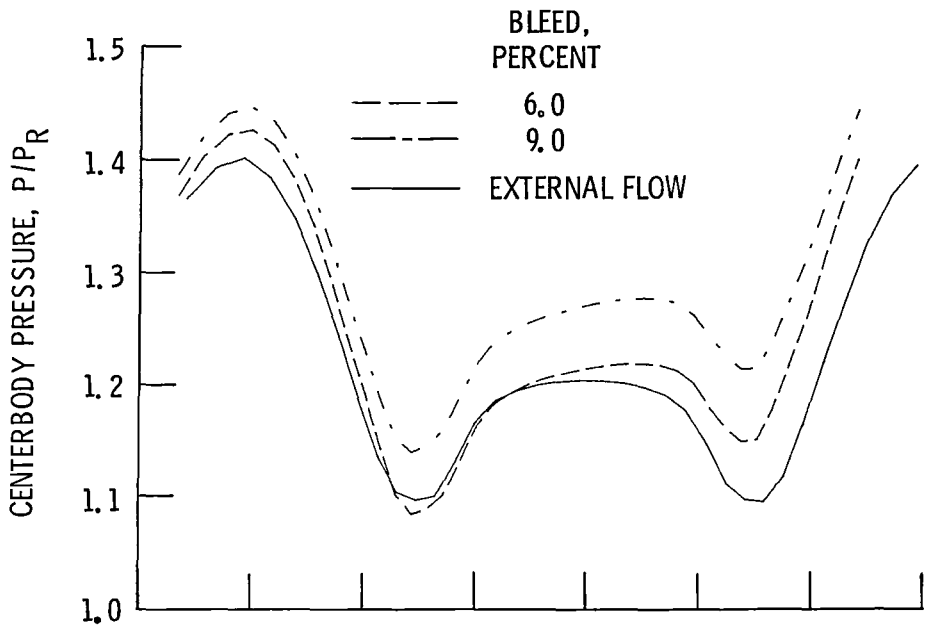

(a) Static pressure.

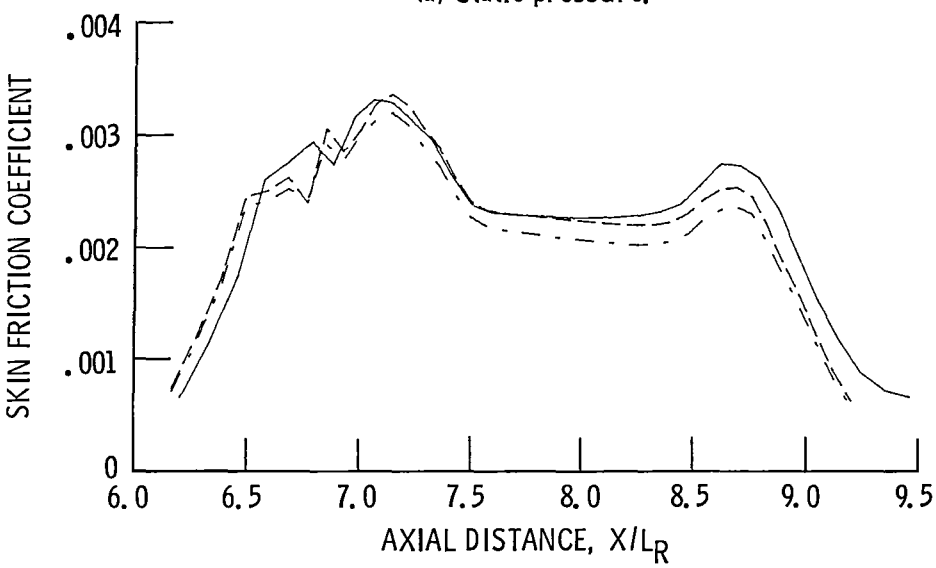

(b) Skin friction coefficient.

Figure 13. - Effect of mass flow removal in AWT test section for 6% blockage, Mach 0.8, 32 000 ft.

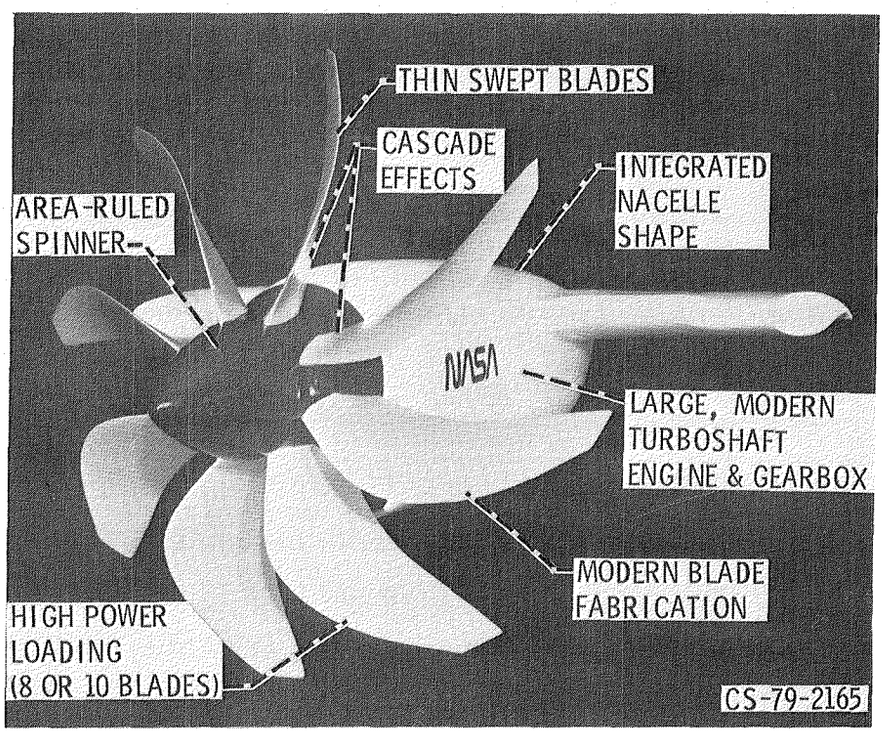

Figure 14. - Typical advanced turboprop propulsion system.

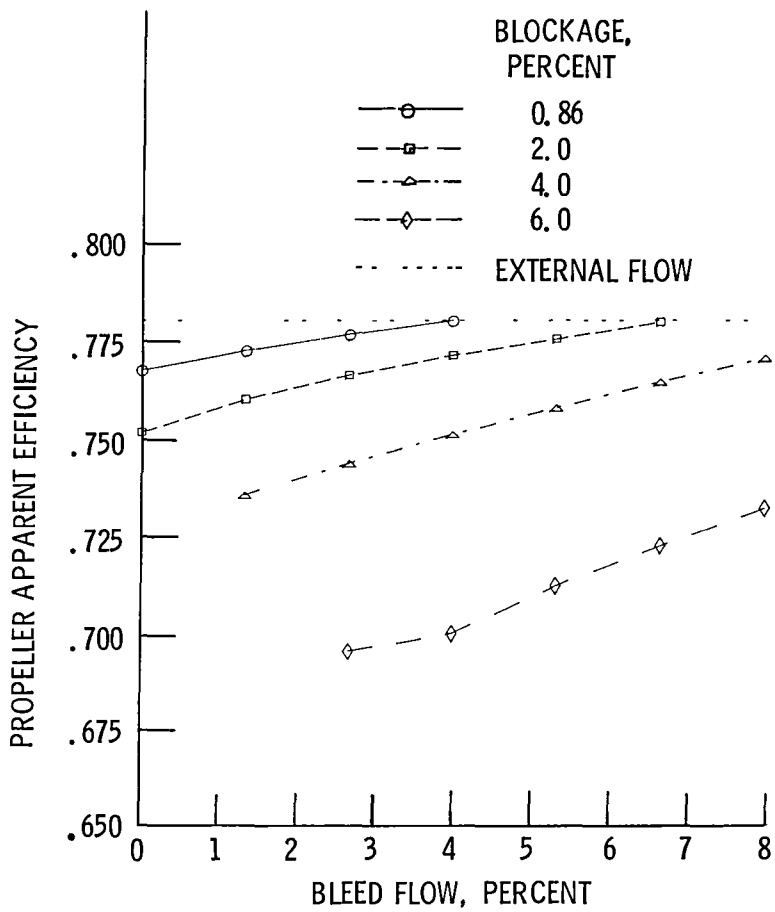

Figure 15. - Effect of mass flow removal on propeller efficiency in AWT at Mach 0.8, 32 000 ft.

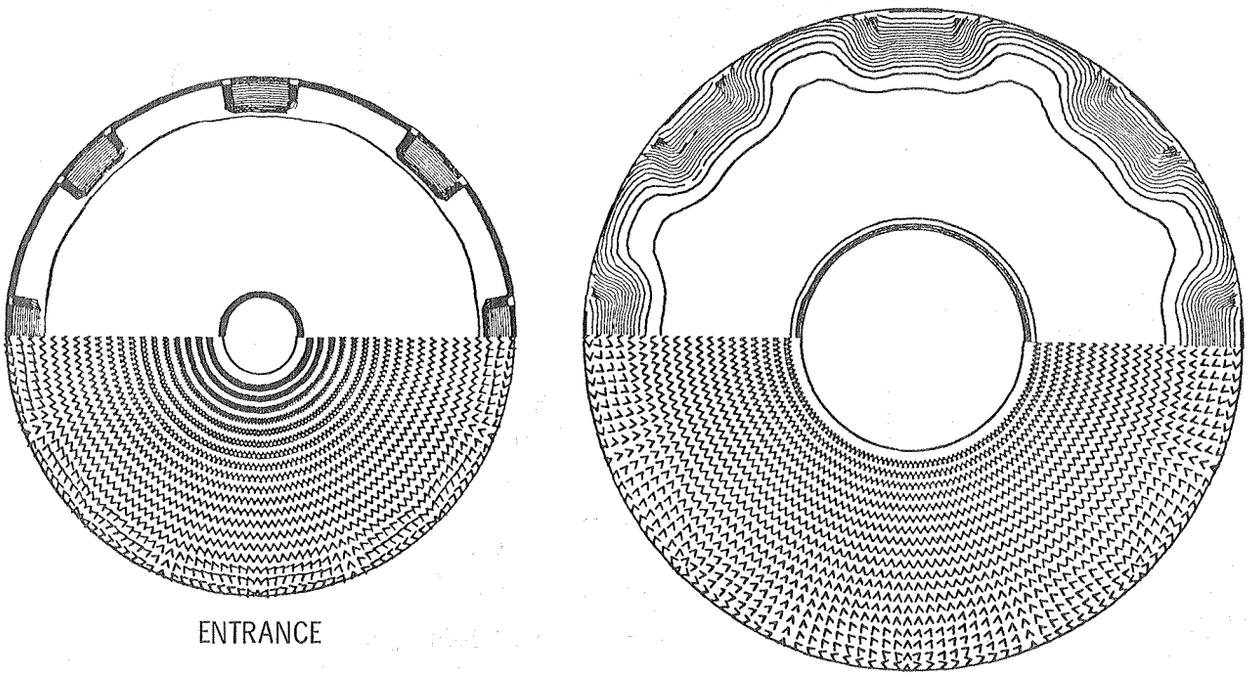

Figure 16. - Effect of inlet distortion due to re-entry flaps on flow in high speed diffuser, Mach 0.8, 32 000 ft, no swirl.

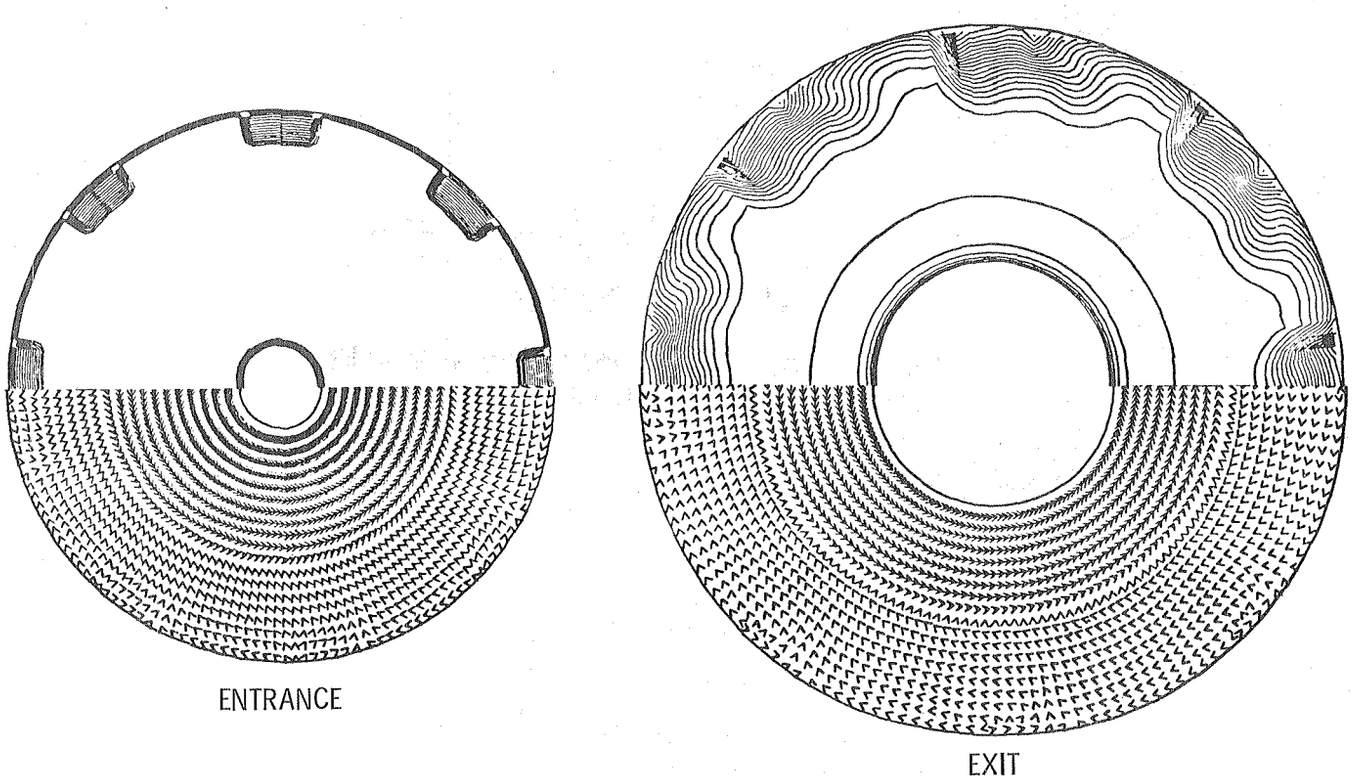

Figure 17. - Effect of inlet distortion due to re-entry flaps on flow in high speed diffuser, Mach 0.8, 32 000 ft, 16% swirl.

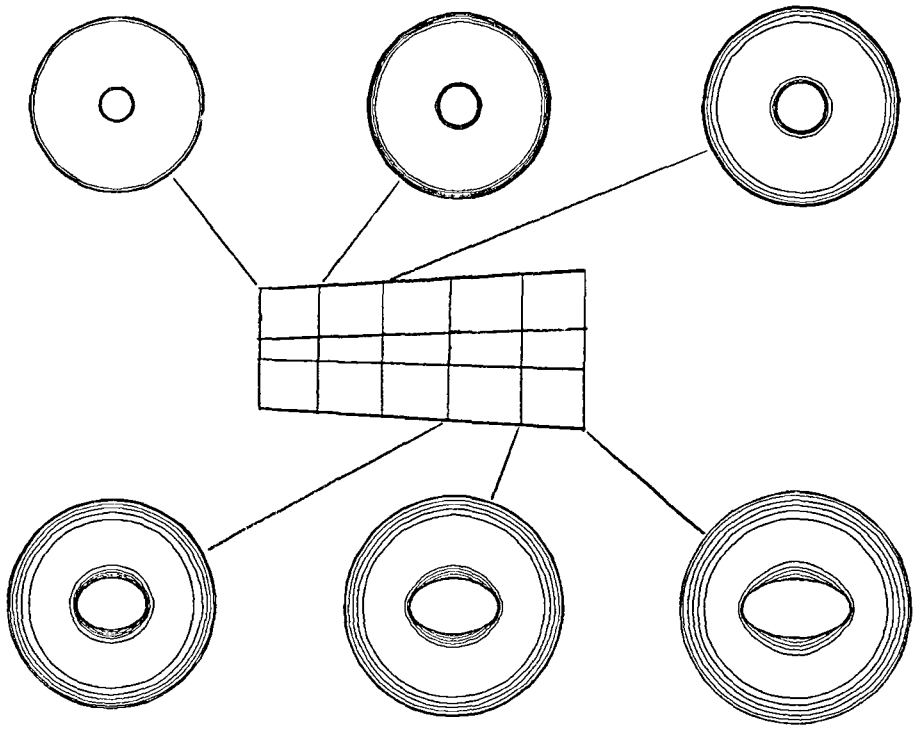

Figure 18. - Effect of change in exhaust scoop shape on axial velocity contours in AWT diffuser.

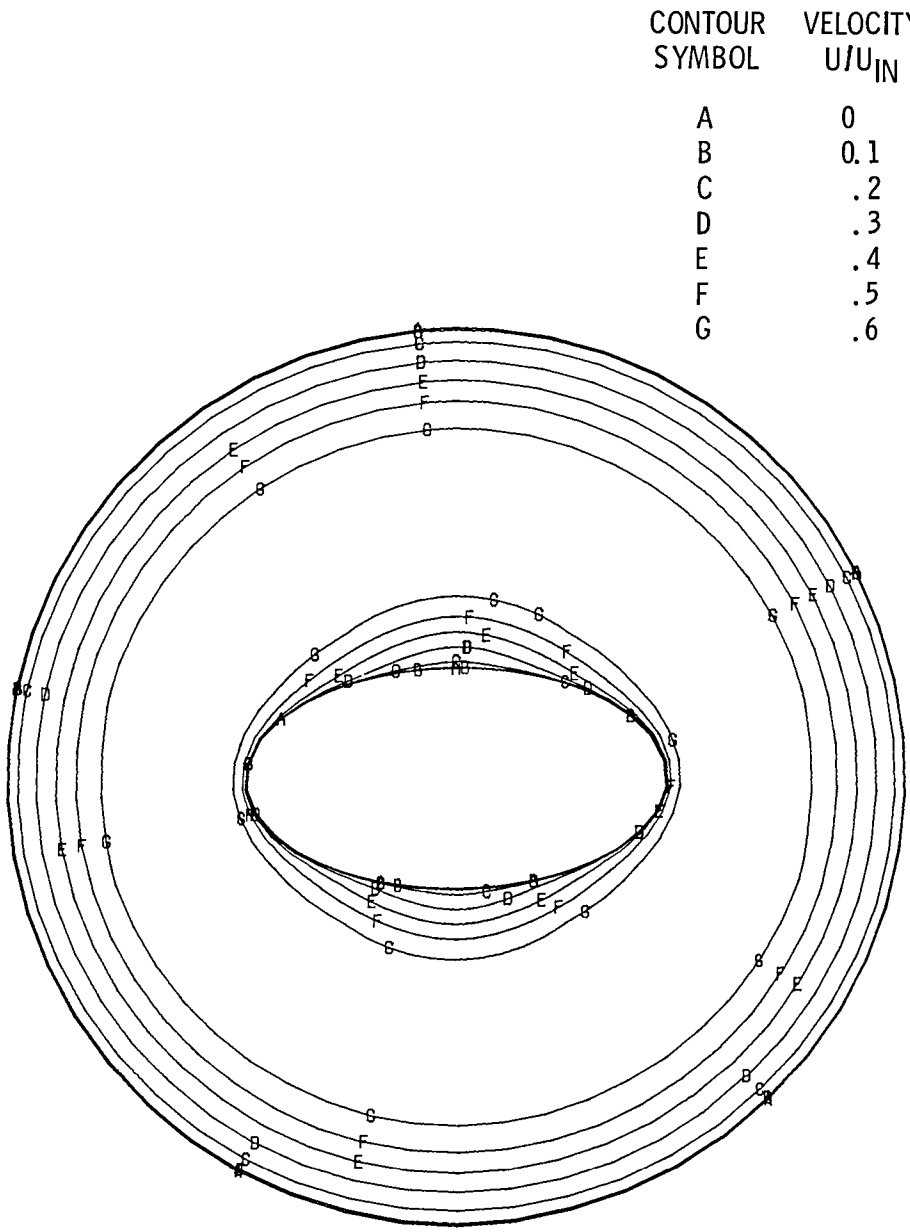

Figure 19. - Axial velocity contours at exit of AWT high speed diffuser.

End of Document